[11] E. C. Sutton, "A superconducting tunnel junction receiver for 230 GHz," *IEEE Trans. Microwave Theory Tech.*, vol. MTT-31, pp. 589–592, July 1983.
[12] Model LTS-3C-4.2 closed-cycle refrigerator, Cryosystems, Westerville, OH, 43081, USA.
[13] Model MU-19-10 doubler, Custom Microwave, Longmont, CO, 80501, USA.
[14] B. M. Thomas, "Design of corrugated conical horns," *IEEE Trans. Antennas Propagat.*, vol. AP-26, pp. 367–372, Mar. 1978.
[15] S. Weinreb, D. L. Fenstermacher, and R. W. Harris, "Ultra-low-noise 1.2 to 1.7 GHz cooled GaAs-FET amplifiers," *IEEE Trans. Microwave Theory Tech.*, vol. MTT-30, pp. 849–853, June 1982.
[16] Model LTE-1138 coolable isolator, Pamtech, Canoga Park, CA, 91304, USA.
[17] D. Rogovin and D. J. Scalapino, "Fluctuation phenomena in tunnel junctions," *Ann. Phys.*, vol. 86, pp. 1–90, July 1974.

**David P. Woody** was born in Santa Monica, CA, on October 30, 1946. He received the B.A. and Ph. D. degrees in physics from the University of California, Berkeley, CA, in 1968 and 1975, respectively.

He worked on balloon-based measurements of the spectrum of the Cosmic Microwave Background from 1971 until 1977. In 1978, he joined the Math, Physics, and Astronomy Department of the California Institute of Technology, Pasadena, where he worked on the development of superconductor–insulator–superconductor tunnel junction millimeter-wave receivers in collaboration with Bell Labs. He is currently a member of the professional staff at the California Institute of Technology's Owens Valley Radio Observatory and is involved in many aspects of the development and operation of the Owens Valley Millimeter Interferometer.

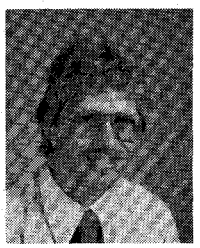

**Ronald E. Miller** was born in Mechanicsburg, PA, on July 19, 1947. He received the Associate in Applied Science degree from the Williamsport Area Community College in 1969. That same year, he joined the Solid State and Physics of Materials Department of Bell Laboratories, where he is now a Member of the Technical Staff. His main research interest is micron and submicron fabrication of thin-film devices.

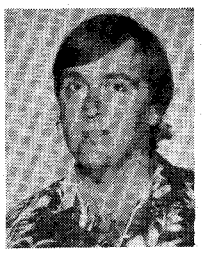

**Michael J. Wengler** was born in Queens, NY, on May 11, 1957. He received the B.A. degree in physics from Swarthmore College, Swarthmore, PA, in 1978. He worked at Bell Labs from 1978 to 1980 on Schottky-diode 115-GHz mixers. Since 1980, he has been a graduate student at Caltech, Pasadena, CA, working on SIS mixer theory and design. He hopes eventually to receive the Ph. D. degree from the Department of Applied Physics at Caltech.

# Field Theory Design of Rectangular Waveguide Broad-Wall Metal-Insert Slot Couplers for Millimeter-Wave Applications

FRITZ ARNDT, SENIOR MEMBER, IEEE, BERND KOCH, HANS-JOACHIM ORLOK, AND NORBERT SCHRÖDER

***Abstract*—A design theory for broad-wall metal-insert slot couplers suitable for an inexpensive and very accurate metal-etching manufacturing technique is described. The method of field expansion into suitable eigenmodes used considers the effects of finite insert thickness and higher order mode interaction at the step discontinuities. Computer-optimized design data for −3-dB couplers in the *Ka*- and *W*-bands are given. The data of the *Ka*-band design are transferable into the *U*- and *V*-bands by suitable frequency scaling calculation. Since the metal-etching technique is also advantageously applicable for couplers in the centimeter wavelength range, optimized design data for *E*-plane slot couplers in the often used *Ku*- and R120-waveguide-bands are included in the tables given. A *Ku*-band metal-etched four-slot coupler prototype achieves a ±1-dB bandwidth of the −3-dB coupling of about 2 GHz, together with −36-dB isolation. The measurements show good agreement with theory.**

Manuscript received May 30, 1984; revised September 18, 1984.

The authors are with the Microwave Department, University of Bremen, Kufsteiner Str., NW 1, D-2800 Bremen 33, West Germany.

## I. INTRODUCTION

COUPLING BY SLOTS over the whole width of the common broad-wall with minor thickness [1] or thicknesses of about one-quarter guide wavelength ("branch guides") [2]–[15] is an attractive technique to design directional couplers with the potential of wide variation of coupling, directivity, input VSWR, and bandwidth values. Although the Reed [4] coupler type has already been successfully applied at millimeter wavelengths [12]—where the approximately $\lambda_{go}/4$ long branch lines are fabricated by assembling and soldering two suitably milled waveguides—for appropriate coupler designs it may often be desirable, however, to make use of the highly accurate and inexpensive metal-etching technique as has been shown recently as an example of metal-insert filters [16], [17]. This

0018-9480/85/0002-0095$01.00 ©1985 IEEE

technique requires coupling wall thicknesses of about $t = 0.05$–$0.2$ mm. The purpose of this paper is to achieve a suitable computer-aided design of such broad-wall slot couplers (see Fig. 1).

The design is based on field expansion into incident and scattered waves of interest. This allows direct inclusion of higher order mode coupling, finite wall thickness, and discontinuity effects at the slots and at the change in the height of the two waveguides. Matching the fields at common interfaces yields the corresponding scattering matrix.

An optimizing computer program varies the coupler parameters until coupling, transmission loss, isolation, and input VSWR correspond to predicted values. So the designer may compromise between different coupler properties, if desired. The evolution strategy method [16], [17] is applied where no differentiation step in the optimization process is necessary. Coupling integrals in the orthogonality relations of the field expansion can be evaluated analytically and only a modest number of waveguide modes is required to achieve satisfactory convergence. This reduces the involved computing time considerably.

Data for optimized *Ka*-band and *W*-band broad-wall slot couplers are given. The *Ka*-band design data are transferable into the *U*- and *V*-bands by suitable frequency scaling calculation as has been proved by exact analysis. The converted coupling sheet metal thicknesses are commercially available ($t = 100$ $\mu$m) for these cases, like the related origin[1] values for the *Ka*-band ($t = 150$ $\mu$m, $t = 190$ $\mu$m, respectively). Since the metal-etching technique is also advantageously applicable for couplers in the centimeter wavelength range, optimized design data for broad-wall slot couplers for the *Ku*- and the R120-waveguide-bands are included in the design tables. Investigations of the influence of tolerances due to etching errors show that the designs are relatively insensitive to that influence. Measured results for a simple metal-etched four-slot 3-dB coupler in the *Ku*-band demonstrate good agreement with theory.

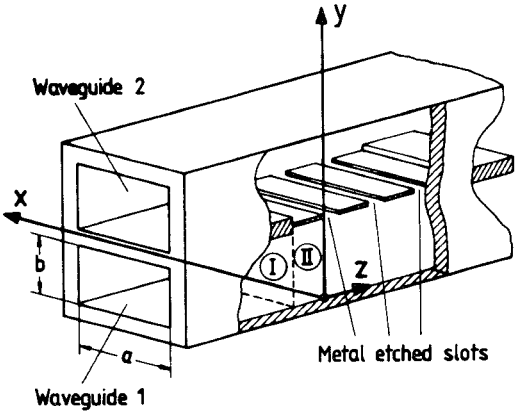


Fig. 1. Broad-wall metal-insert slot coupler with insert thicknesses of about $t = 50$–$200$ $\mu$m suitable for metal-etching manufacturing technique.

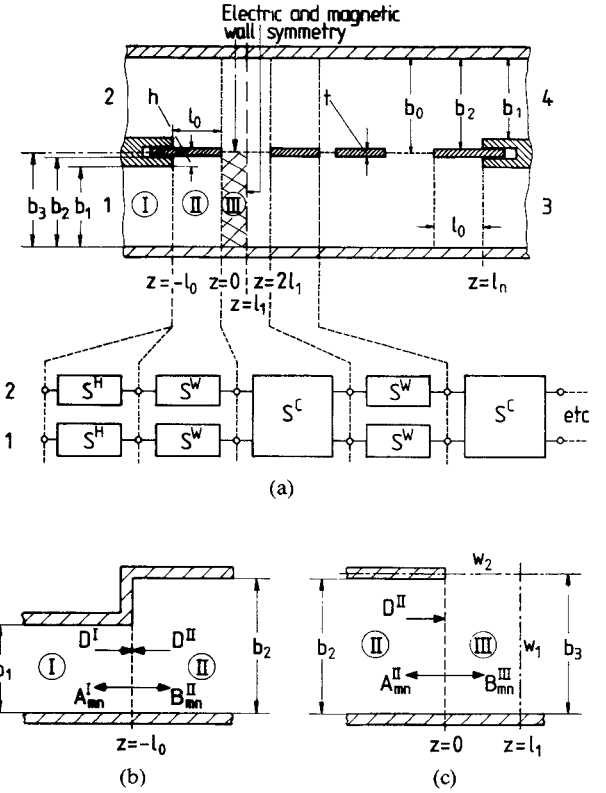


Fig. 2. Configuration for the field-theory treatment. (a) Waveguides together with the metal insert containing the metal-etched coupling slots. The scattering matrices are $S^H$ discontinuity change in waveguide height (two-port), $S^W$ (homogeneous) waveguide section (two-port), and $S^C$ coupling slot-section including finite wall thickness (four-port). (b) Step discontinuity at the change in waveguide height at $z = -l_0$. (c) One-quarter section of the symmetric total coupling slot section ($z = 0, \cdots, z = 2l_1$, cf., Fig. 2(a)) with four boundary cases, (electric and/or magnetic wall at $w_1$ and/or $w_2$). Instead of $b_0$ in the upper right quarter of Fig. 2(a), read $b_3$.

## II. Theory

For the computer-aided design of broad-wall slot couplers (see Fig. 1) the modal expansion technique [15]–[21] is applied. Normal eigenmodes are chosen so as to satisfy boundary conditions at the discontinuity. The technique proves to be ideally suited to computers, involving mainly the solution of sets of simultaneous linear equations. In contrast to network theory synthesis methods which have attained a high standard for the common branch-guide couplers [2]–[14], interaction effects of higher order modes between discontinuities (including the change in waveguide height and the coupling slot section with finite wall thickness) are taken into account. The inclusion of these effects has turned out to be important for this kind of broad-wall slot couplers.

A $TE_{10}$-wave incident in port 1, shown in Fig. 2(a), excites longitudinal section $TE^x_{mn}$-waves [18], [19] at all step discontinuities. As in [15]–[17], therefore, for each typical homogeneous subregion $\nu$ = I, II, and III (cf., Fig. 2(a)) the fields [18]

$$\boldsymbol{E}^{(\nu)} = -j\omega\mu\nabla \times \Pi^{(\nu)}_{hx} \qquad \boldsymbol{H}^{(\nu)} = \nabla \times \nabla \times \Pi^{(\nu)}_{hx} \quad (1)$$

are derived from the $x$-component of the magnetic Hertzian vector potential $\Pi_h$, which is assumed to be a sum of suitable eigenmodes satisfying the vector Helmholtz equation and the boundary conditions.

For the investigation of the discontinuity at the change in waveguide height at $z=-l_0$ (Fig. 2(a) and (b)), the Hertzian vector potentials for subregions $\nu=\mathrm{I}, \mathrm{II}$ are assumed to be

$$\Pi_{hx}^{I}=\sum_{n=0}^{N}\left(A_{mn}^{I}e^{+jk_{zmn}^{\mathrm{I}}(z+l_0)}+D^{I}\delta_{qn}e^{-jk_{zmn}^{\mathrm{I}}(z+l_0)}\right)\cdot\sin k_x x\cos k_y^{\mathrm{I}}y$$

$$\Pi_{hx}^{II}=\sum_{n=0}^{N}\left(B_{mn}^{II}e^{-jk_{zmn}^{\mathrm{II}}(z+l_0)}+D^{\mathrm{II}}\delta_{qn}e^{+jk_{zmn}^{\mathrm{II}}(z+l_0)}\right)\cdot\sin k_x x\cos k_y^{\mathrm{II}}y \quad (2)$$

where

$$k_x=\frac{m\pi}{a},\ k_y^{\mathrm{I}}=\frac{n\pi}{b_1},\ k_y^{II}=\frac{n\pi}{b_2},\ k_{zmn}^{\nu 2}=k^2-k_x^2-k_y^{\nu 2}$$

with $k^2=\omega^2\mu\epsilon$, $\delta_{qn}$ is the Kronecker delta, $N$ is the number of eigenmodes considered, $D^{\mathrm{I}}, D^{\mathrm{II}}$ are the amplitudes of the exciting $\mathrm{TE}_{mq}^{x}$-wave, and $A_{mn}, B_{mn}$ are the unknown amplitude coefficients of the eigenwaves excited at the discontinuity. In (2), a summation of the $A_{mn}, B_{mn}$ with regard to the index $m$ is not necessary, a change in the mode order $m$ does not occur since there are no structural variations in the $x$-direction (Figs. 1 and 2).

By matching of the tangential field components at the common interfaces $E_y^{(\mathrm{I})}=E_y^{(\mathrm{II})}$ $(y\epsilon(0,b_1))$, $E_y^{(\mathrm{II})}=0$ $(y\epsilon(b_1,b_2))$, $H_x^{(\mathrm{I})}=H_x^{(\mathrm{II})}$ $(y\epsilon(0,b_1))$, $H_y^{(\mathrm{I})}=H_y^{(\mathrm{II})}$ $(y\epsilon(0,b_1))$ across the step discontinuity at $z=-l_0$, a process which may be simplified using (1), by the conditions

$$\Pi_{hx}^{(\mathrm{I})}=\Pi_{hx}^{\mathrm{II}}\big|_{z=-l_0} \qquad y\in(0,b_1)$$

$$\frac{\delta\Pi_{hx}^{\mathrm{II}}}{\delta z}=\begin{cases}\left.\dfrac{\delta\Pi_{hx}^{\mathrm{I}}}{\delta z}\right|_{z=-l_0} & y\in(0,b_1)\\ 0 & y\in(b_1,b_2)\end{cases} \quad (3)$$

and utilizing the orthogonal property of the modes [18], the still unknown coefficients $A_{mn}^{\mathrm{I}}, B_{mn}^{\mathrm{II}}$ in (2) can be related to each other

$$D^{\mathrm{I}}\delta_{qn}+A_{mn}^{\mathrm{I}}=\sum_{k=0}^{N}\left(D^{\mathrm{II}}\delta_{qk}+B_{mk}^{\mathrm{II}}\right)e_{nk}$$

$$\sum_{n=0}^{N}\left(D^{\mathrm{I}}\delta_{qn}-A_{mn}^{\mathrm{I}}\right)k_{zmn}^{\mathrm{I}}f_{kn}=\left(-D^{\mathrm{II}}\delta_{qn}+B_{mk}^{\mathrm{II}}\right)k_{zmk}^{\mathrm{II}}. \quad (4)$$

The coupling integrals $e_{nk}$, $f_{nk}$ due to the orthogonal property of the modes are elucidated in the Appendix. Using the matrix notation and considering successively the exitation by the $\mathrm{TE}_{mq}^{x}$-waves with the amplitudes $D^{\mathrm{I}}=D^{\mathrm{II}}=1$ in the subregions I and II, (4) may be written in the form of the scattering matrix $(S^H)$ of the discontinuity at the change in waveguide height

$$(S^H)=\begin{pmatrix}(S_{11}^H) & (S_{12}^H)\\ (S_{21}^H) & (S_{22}^H)\end{pmatrix} \quad (5)$$

after suitable normalization so that the power carried by a given wave is proportional to the square of the absolute value of the amplitude coefficient [18]. The scattering matrix elements of (5), each of which is a matrix of $N$th dimension, are given in the Appendix.

For the investigation of the discontinuity at the coupling slot section at $z=0$ (Fig. 2(a) and (c)) the Hertzian vector potentials for subregions $\nu=\mathrm{II},\mathrm{III}$ are assumed to be

$$\Pi_{hx}^{\mathrm{II}}=\sum_{n=0}^{N}\left(A_{mn}^{\mathrm{II}}e^{+jk_{zmn}^{\mathrm{II}}z}+D^{\mathrm{II}}\delta_{qn}e^{-jk_{zmn}^{\mathrm{II}}z}\right)\sin k_x x\cos k_y^{\mathrm{II}}y$$

$$\Pi_{hx}^{\mathrm{III}}=\sum_{n=0}^{N}B_{mn}^{\mathrm{III}}\sin k_x x\cos k_y^{\mathrm{III}}y\ \Psi_{mn}^{ci}(z) \quad (6)$$

where

$$k_y^{\mathrm{III}}=\frac{n\pi}{b_3},\ k_y^{\mathrm{III}}=\frac{(2n+1)}{2}\cdot\frac{\pi}{b_3}$$

respectively (cf., Appendix).

The standing-wave expression $\Psi_{mn}^{ci}(z)$ (cf., Appendix) is due to the fact that the calculation of the symmetric total coupling slot section ($z=0,\cdots,z=2l_1$, Fig. 2(a))—including the discontinuity effect of the finite wall thickness $t$—may be simplified considerably by consequent application of the even and odd normal mode principle [3]. This leads to the one-port equivalent of the one-quarter section (III) (cf., Fig. 2(c)) including four boundary cases $c1,\cdots,c4$ (electric and/or magnetic wall at $w_1$ and/or $w_2$) if a unit wave amplitude $D^{\mathrm{II}}$ is incident from subregion II (cf., Appendix).

By matching of the tangential field components at the common interfaces across the step discontinuity at $z=0$, the coefficients $A_{mn}^{\mathrm{II}}$, $B_{mn}^{\mathrm{III}}$ in (6) can be related to each other, analogously to (4), for each of the four boundary cases. The corresponding equations are given in the Appendix.

The four-port matrix $(S^C)$ of the symmetric total coupling slot section ($z=0,\cdots,z=2l_1$, Fig. 2(a))

$$(S^C)=\begin{pmatrix}(S_{11}^C) & (S_{12}^C) & (S_{13}^C) & (S_{14}^C)\\ (S_{12}^C) & (S_{11}^C) & (S_{14}^C) & (S_{13}^C)\\ (S_{13}^C) & (S_{14}^C) & (S_{11}^C) & (S_{12}^C)\\ (S_{14}^C) & (S_{13}^C) & (S_{12}^C) & (S_{11}^C)\end{pmatrix} \quad (7)$$

is then given by

$$\begin{aligned}(S_{11}^C)&=\frac{1}{4}\left[(S_{1p}^{c1})+(S_{1p}^{c2})+(S_{1p}^{c3})+(S_{1p}^{c4})\right]\\ (S_{12}^C)&=\frac{1}{4}\left[(S_{1p}^{c1})+(S_{1p}^{c2})-(S_{1p}^{c3})-(S_{1p}^{c4})\right]\\ (S_{13}^C)&=\frac{1}{4}\left[(S_{1p}^{c1})-(S_{1p}^{c2})+(S_{1p}^{c3})-(S_{1p}^{c4})\right]\\ (S_{14}^C)&=\frac{1}{4}\left[(S_{1p}^{c1})-(S_{1p}^{c2})-(S_{1p}^{c3})+(S_{1p}^{c4})\right]\end{aligned} \quad (8)$$

where $S_{1p}^{ci}$ is the input reflection coefficient of the one-port equivalent of the one-quarter section III for the boundary cases $c1$, $c2$, $c3$, and $c4$, respectively (cf., Appendix).

TABLE I
COMPUTER-OPTIMIZED DESIGN DATA FOR $E$-PLANE METAL INSERT −3-dB COUPLERS IN THE $KA$-BAND (WR28-HOUSING: 7.122 MM × 3.556 MM)

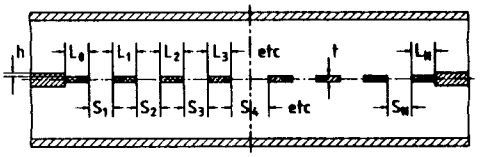


| Number of Slots N | Metal Insert Thickness t (mm) | Slot Lengths (mm) $S_1=S_N$ | $S_2=S_{N-1}$ | $S_3=S_{N-2}$ | $S_4=S_{N-3}$ | $S_5=S_{N-4}$ | Intermediate Lengths of Waveguide Section (mm) $L_0=L_N$ | $L_1=L_{N-1}$ | $L_2=L_{N-2}$ | $L_3=L_{N-3}$ | $L_4=L_{N-4}$ | Height h (mm) | Midband Frequency (GHz) | ± 1dB Bandwidth of the -3dB Coupling (GHz) | Isolation (dB) | Return Loss (dB) |
|---|---|---|---|---|---|---|---|---|---|---|---|---|---|---|---|---|
| 5 | 0.19 | 0.123 | 0.528 | 0.376 | | | 1) | 2.746 | 1.902 | | | 0 | 31.7 | 4 | 40 | 39 |
| 5 2) | 0.15 | 0.112 | 0.532 | 0.554 | | | 1) | 2.639 | 1.943 | | | 0 | 33 | 4.5 | 40 | 39 |
| 5 3) | 0.085 | 0.153 | 1.261 | 0.092 | | | 0.765 | 1.730 | 0.192 | | | 0.225 | 34 | 4.5 | 30 | 30 |

1) To avoid higher order mode coupling effects, for practical designs, $L_0 = L_N$ should be about two guide-wavelengths long (cf., Fig. 3(d)).
2) Results shown in Fig. 4.
3) Results shown in Fig. 3(a).

Similar to [21], the overall four-port scattering matrix of the total coupler (Fig. 2(a)) is calculated by suitable direct combination of all single scattering matrices $(S^H)$, $(S^C)$, and $(S^W)$, the two-port scattering matrix of a homogeneous waveguide section. Although the corresponding equations are somewhat voluminous, compared with the commonly used multiplication of transmission matrices, this procedure preserves numerical accuracy, since the direct combination of scattering matrix parameters contains exponential functions with only negative argument.

For computer optimization, the expansion into five eigenmodes at each step discontinuity (change in height and bifurcation at the coupling slot) and four eigenmodes along each intermediate homogeneous waveguide section has turned out to be sufficient. The final design data are provided by expansion into eighteen eigenmodes.

## III. DESIGN

As has already been introduced for metal-insert filters [16], [17], the computer-aided design is carried out by an optimizing program applying the evolution strategy method, which varies the input parameters until the desired coupler scattering matrix values for a given bandwidth are obtained. An error function $F(\bar{x})$ to be minimized is defined

$$F(\bar{x}) = \sum_{i=1}^{I} \left( \frac{S_{11D}}{S_{11}(f_i)} \right)^2 + \left( \frac{S_{12D}}{S_{12}(f_i)} \right)^2 + \left( \frac{S_{13D}}{(S_{13}(f_i) + S_{13T})} \right)^2 + \left( \frac{S_{14D}}{(S_{14}(f_1) + S_{14T})} \right)^2 \overset{!}{=} \text{Min} \tag{9}$$

where $I$ is the number of frequency sample points $f_i$; $S_{11D}$, $S_{12D}$, $S_{13D}$, $S_{14D}$ are the desired given input reflection, isolation, transmission, and coupling coefficients, in decibels, like $S_{11}$, $S_{12}$, $S_{13}$, and $S_{14}$, which are the calculated scattering coefficients of the coupler (Fig. 1) at the frequency $f_i$; $S_{13T}$ and $S_{14T}$ are the given tolerated deviations in decibels of the desired transmission and coupling coefficients within a certain bandwidth range. $S_{13}$ and $S_{14}$ are the calculated scattering coefficients of the coupler (Fig. 1) at the frequency $f_i$; $S_{13T}$ and $S_{14T}$ are the given tolerated deviations of the desired transmission and coupling coefficients within a certain bandwidth range. For desired waveguide housing dimensions, thickness $t$ of the broad-wall coupling metal insert, and number of coupling slots, the parameters $\bar{x}$ to be optimized (Table I) are the slot and the intermediate coupling wall lengths. The total time for the optimization of one set of coupler parameters, e.g., for a five-slot coupler, was about 60 min with the SIEMENS-7880 computer at the University of Bremen.

## IV. RESULTS

The influence of the step height $h$ at the discontinuities $z = -l_0$, $z = l_n$, Fig. 2(a) (change in waveguide height between the common broad wall of the waveguides and the coupling metal insert containing the metal-etched slots) is demonstrated in Fig. 3(a)–(d) as an example of a $Ka$-band five-slot coupler with a coupling sheet-metal thickness $t =$ 85 $\mu$m. Fig. 3 (a) shows the magnitude of the scattering coefficients $S_{11}$, $S_{12}$, $S_{13}$, and $S_{14}$ in decibels (return loss, isolation, transmission, and coupling coefficient) as a function of frequency of the computer-optimized coupler with a step height of $h = 0.225$ mm included in the optimization process, as well as the length $l_0 = 0.77$ mm of the intermediate waveguide section towards the first or the last slot (Fig. 2(a)). Fig. 3(b) and (c), where $h$ is chosen to be about four ($b$) and six times ($c$) the height given in Fig. 3(a), demonstrate the distortion of the coupler behavior due to the higher order mode excitation at the step discontinuities

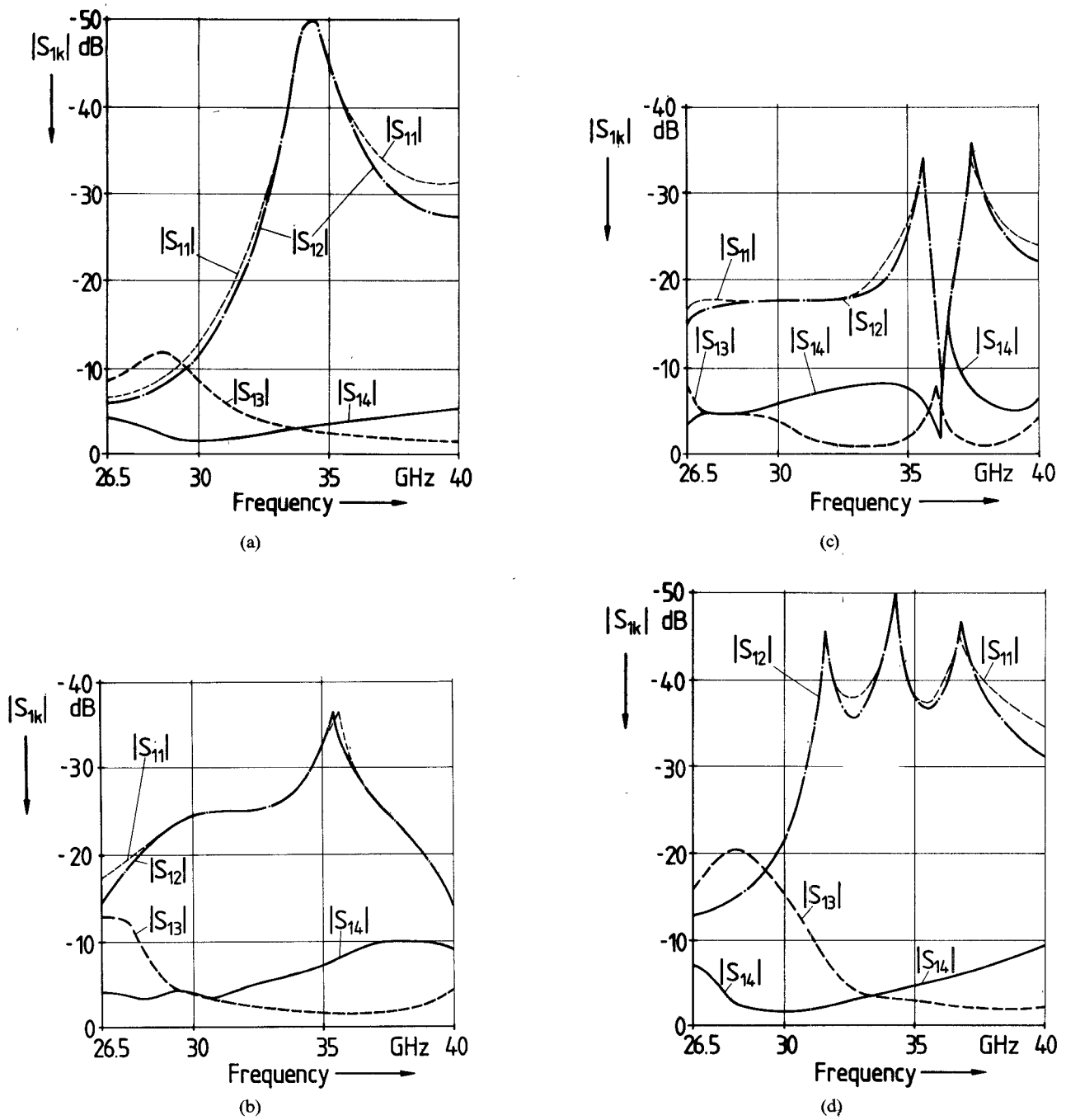


Fig. 3. Magnitude of the scattering coefficients $S_{11}$, $S_{12}$, $S_{13}$, and $S_{14}$ in decibels (return loss, isolation, transmission, and coupling coefficient) as a function of frequency for a five-slot coupler in the *Ka*-band to demonstrate the influence of the step height $h$ at the discontinuities $z = -l_0$, $z = l_n$, Fig. 2(a) (change in waveguide height of the common broad wall). Coupling sheet-metal thickness $t = 85$ $\mu$m. (a) Optimized coupler, $h = 0.225$ mm, length $l_0$ of the intermediate waveguide section towards the first or last slot $l_0 = 0.77$ mm (included in the optimization process) (cf., Table I), (b) coupler of Fig. 3(a), but $h = 0.9$ mm, $l_0 = 0.77$ mm, (c) coupler of Fig. 3(a), but $h = 1.35$ mm, $l_0 = 0.77$ mm, (d) coupler of Fig. 3(a) ($h = 0.225$ mm), but $l_0 = 22.5$ mm.

$z = -l_0$, $z = l_n$ for increasing step height $h$. This influence may be reduced, however, by assuming an intermediate waveguide section of sufficient length $l_0$, e.g., about two guide wavelengths long at midband frequency (Fig. 3(d)) where the excited higher order modes die down to a negligible value.

In order to achieve a better broad-band behavior than shown in Fig. 3(a), the previous results are utilized by choosing a broad-wall slot coupler with negligible step discontinuity height $h$ at $z = -l_0$, $z = l_n$ (Fig. 2(a)) to be optimized in the further designs. This may be achieved by suitable mechanical construction, e.g., by a smooth transition together with a suitable length $l_0$ of the intermediate waveguide section towards the first and last slot. Fig. 4 shows the result of an optimized five-slot coupler (cf., Table I) in the *Ka*-band, where $h$ is assumed to be negligible. The analogy to the coupler behavior in Fig. 3(d) is obvious. This design yields a $-3$-dB $\pm$ 1-dB coupling bandwidth of about 5 GHz (relative bandwidth about 15 percent) with about 40-dB return loss and isolation.

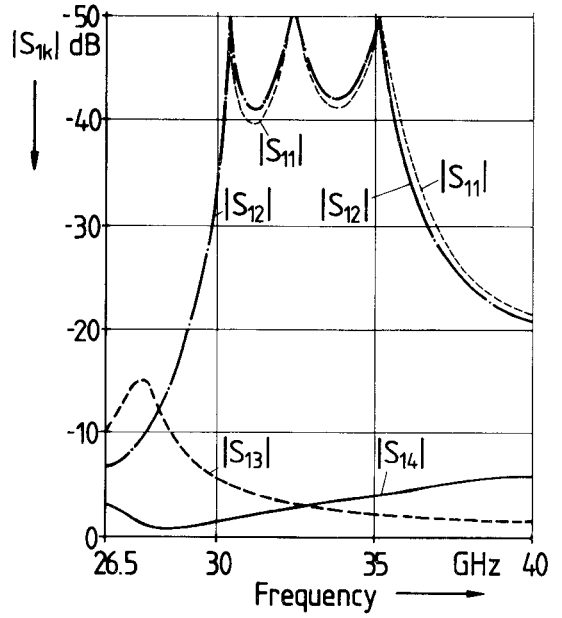


Fig. 4. Magnitude of the scattering coefficients as a function of frequency for a computer-optimized five-slot coupler (cf., Table I) in the *Ka*-band. Coupling sheet-metal thickness $t = 150$ $\mu$m, step height $h = 0$ mm.

The *Ka*-band broad-wall slot coupler design data (cf., Table I) may be transformed by suitable frequency scaling calculation into other common frequency bands covering the same relative frequency range, e.g, the *U*-band (40–60 GHz) and the *V*-band (50–75 GHz). As has been proved by exact analysis, the transformation of all geometrical dimensions (including the coupling sheet-metal thickness $t$) with the related cutoff frequency ratio ($\lambda_{c\text{new}}/\lambda_{c\,Ka\text{-band}}$) yields only slight deviation of the coupler behavior compared with the optimized original results of the *Ka*-band. The coupling sheet-metal thickness scaled down to the *U*-band ($t \approx 100$ $\mu$m) and *V*-band ($t \approx 100$ $\mu$m) from the original *Ka*-band value ($t = 150$ $\mu$m, $t = 190$ $\mu$m, respectively) are commercially available, too. For higher frequency bands, like the *W*-band, however, truncation errors, e.g., concerning the metal-insert thickness, would lead to a noticeable influence on the coupler behavior. For the *W*-band, therefore, optimization data are given in Table II. The curves of an optimized *W*-band broad-wall five-slot coupler (cf., Table II), for example, are shown in Fig. 5. The $\pm 1$-dB bandwidth of the $-3$-dB coupling is about 9 GHz (relative bandwidth about 10 percent) with more than 30-dB return loss and isolation.

Since the metal-etching technique is also advantageously applicable for accurate and inexpensive production of couplers in the centimeter wavelength range, Tables III and IV yield optimized design data for *E*-plane couplers in the *Ku*-band and in the also often-used R120-waveguide-band (10–15 GHz). The latter design data include $-4.77$-dB couplers for application as power dividers in three parts. Fig. 6 shows the magnitude of the scattering coefficients $S_{12}$, $S_{13}$, and $S_{14}$ of a simple broad-wall four-slot coupler in the *Ku*-band which achieves, nevertheless, an absolute $\pm 1$-dB bandwidth of about 2 GHz (relative bandwidth about 12 percent) of the $-3$-dB coupling with about 36-dB return loss and isolation (the curve for $|S_{11}|$ is omitted for clearness because it is nearly identical with $|S_{12}|$).

To demonstrate the influence of etching errors on the coupler behavior, Fig. 6 includes the corresponding $|S_{12}|$ results if maximum etching errors of $\Delta l = +70$ $\mu$m (all coupling slot lengths are 70 $\mu$m longer, curve 2) and of $\Delta l = -70$ $\mu$m (all slot lengths shorter, curve 3) are assumed for a worst-case example. These errors lead to a noticeable deviation of the isolation (and return-loss) behavior, the minimum value is more than 32 dB, however, in spite of these hypothetical relatively high etching errors. Normally, the metal etching accuracy is better than $\pm 40$ $\mu$m, as has been proved by metal-insert filter designs [16], [17] and by production of simple broad-wall slot coupler prototypes. Fig. 7 shows the photograph of the coupling metal insert containing the four metal-etched coupling slots of the fabricated simple *Ku*-band coupler of Fig. 6, Table IV. The material of the 150-$\mu$m-thick insert is 99.9-percent pure copper; the measured deviation from the $-3$-dB coupling insertion loss due to copper losses is less than 0.1 dB. The measured results (Fig. 6) show good agreement with theory.

## V. Conclusion

Broad-wall metal-insert slot couplers achieve coupler designs suitable for the inexpensive and very accurate metal etching technique advantageously applied recently as an example of waveguide-integrated millimeter-wave filters. A suitable computer-aided design of such filters is based on the method of field expansion in appropriate eigenmodes which allows inclusion of finite metal thicknesses and the higher order mode interaction at the step discontinuities. Computer-optimized design data for three- to seven-slot couplers with commercially available metal-insert thicknesses of 100, 150, and 190 $\mu$m are given for the *Ka*- and the *W*-bands. The design data for the *Ka*-band are transferable into the *U*- and *V*-bands by suitable frequency scaling calculation. Since the metal-etching technique is also advantageously applicable in the centimeter-wave range, optimized design data for broad-wall slot couplers for the *Ku*- and R120-waveguide-band are included in the results. Measurements at a simple four-slot *Ku*-band coupler prototype show good agreement with theory.

## Appendix

*Coupling Integrals in (4)*

$$e_{nk} = \frac{2}{b_1}\int_0^{b_1} \frac{1}{\sqrt{1+\delta_{0k}}}\,\frac{1}{\sqrt{1+\delta_{0n}}}\cos\left(\frac{k\pi}{b_2}y\right)\cos\left(\frac{n\pi}{b_1}y\right)dy$$

$$f_{kn} = \frac{2}{b_2}\int_0^{b_1} \frac{1}{\sqrt{1+\delta_{0k}}}\,\frac{1}{\sqrt{1+\delta_{0n}}}\cos\left(\frac{k\pi}{b_2}y\right)\cos\left(\frac{n\pi}{b_1}y\right)dy. \quad \text{(A1)}$$

TABLE II
COMPUTER-OPTIMIZED DESIGN DATA FOR *E*-PLANE METAL INSERT −3-dB COUPLERS IN THE *W*-BAND (WR10-HOUSING: 2.54 MM×1.27 MM)

| Number of Slots N | Metal Insert Thickness t (mm) | Slot Lengths (mm) | | | | | Intermediate Lenghts of Waveguide Section (mm) | | | | | Height h (mm) | Midband Frequency (GHz) | ± 1dB Bandwidth of the -3dB Coupling (GHz) | Isolation (dB) | Return Loss (dB) |
|---|---|---|---|---|---|---|---|---|---|---|---|---|---|---|---|---|
| | | $S_1=S_N$ | $S_2=S_{N-1}$ | $S_3=S_{N-2}$ | $S_4=S_{N-3}$ | $S_5=S_{N-4}$ | $L_0=L_N$ | $L_1=L_{N-1}$ | $L_2=L_{N-2}$ | $L_3=L_{N-3}$ | $L_4=L_{N-4}$ | | | | | |
| 3 | 0.1 | 0.146 | 0.536 | | | | 1) | 0.865 | | | | 0 | 89 | 9 | 30 | 30 |
| 3 | 0.15 | 0.168 | 0.579 | | | | 1) | 0.799 | | | | 0 | 89 | 9 | 29 | 28 |
| 5[2] | 0.15 | 0.104 | 0.152 | 0.271 | | | 1) | 0.725 | 0.388 | | | 0 | 90.3 | 10 | 33 | 34 |
| 7 | 0.15 | 0.101 | 0.145 | 0.106 | 0.133 | | 1) | 0.694 | 0.209 | 0.200 | | 0 | 94 | 5 | 38 | 38 |

1) cf., footnote Table I.
2) Results shown in Fig. 5.

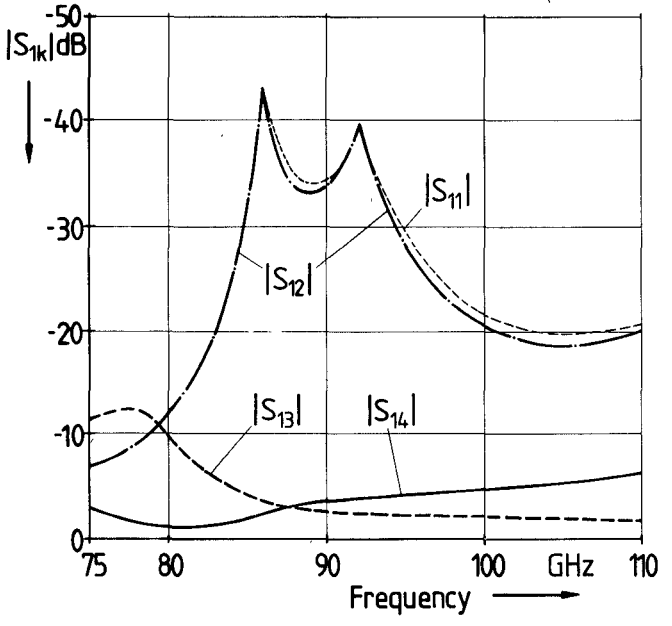


Fig. 5. Magnitude of the scattering coefficients as a function of frequency for a computer optimized *W*-band five-slot coupler (cf., Table II). Coupling sheet-metal thickness $t = 150\ \mu$m, step height $h = 0$ mm.

TABLE III
COMPUTER-OPTIMIZED DESIGN DATA FOR *E*-PLANE METAL INSERT −3-dB COUPLERS IN THE *KU*-BAND (WR62-HOUSING: 15.79 MM×7.899 MM)

| Number of Slots N | Metal Insert Thickness t (mm) | Slot Lengths (mm) | | | | | Intermediate Lenghts of Waveguide Section (mm) | | | | | Height h (mm) | Midband Frequency (GHz) | ± 1dB Bandwidth of the -3dB Coupling (GHz) | Isolation (dB) | Return Loss (dB) |
|---|---|---|---|---|---|---|---|---|---|---|---|---|---|---|---|---|
| | | $S_1=S_N$ | $S_2=S_{N-1}$ | $S_3=S_{N-2}$ | $S_4=S_{N-3}$ | $S_5=S_{N-4}$ | $L_0=L_N$ | $L_1=L_{N-1}$ | $L_2=L_{N-2}$ | $L_3=L_{N-3}$ | $L_4=L_{N-4}$ | | | | | |
| 4 | 0.19 | 0.198 | 3.623 | | | | 1) | 4.315 | 0.914 | | | 0 | 17 | 1.8 | 40 | 40 |
| 4[2] | 0.19 | 0.330 | 2.890 | | | | 1) | 3.750 | 0.370 | | | 0 | 16 | 2 | 37 | 37 |
| 6 | 0.19 | 0.336 | 2.720 | 0.163 | | | 1) | 4.311 | 0.611 | 2.001 | | 0 | 16.6 | 2 | 35 | 35 |
| 7 | 0.19 | 0.198 | 1.320 | 0.476 | 1.814 | | 1) | 4.346 | 1.985 | 0.865 | | 0 | 16.6 | 2 | 40 | 40 |
| 9 | 0.19 | 0.371 | 1.773 | 0.112 | 0.159 | 0.127 | 1) | 4.208 | 0.542 | 4.141 | 2.143 | 0 | 16.7 | 2 | 40 | 40 |
| 5 | 0.19 | 0.339 | 2.801 | 0.205 | | | 1.7 | 3.842 | 0.426 | | | 0.5 | 15.3 | 1.3 | 30 | 30 |
| 7 | 0.19 | 0.200 | 0.750 | 0.640 | 2.400 | | 0.95 | 3.950 | 1.960 | 0.900 | | 2 | 14.7 | 1 | 32 | 32 |

1) cf., footnote Table I.
2) Results shown in Fig. 6.

TABLE IV
COMPUTER-OPTIMIZED DESIGN DATA FOR $E$-PLANE METAL INSERT COUPLERS IN THE R120-BAND
(WR75-HOUSING: 19.05 MM × 9.525 MM)

| Coupling (dB) | Number of Slots N | Metal Insert Thickness t (mm) | Slot Lengths (mm) | | | | | Intermediate Lenghts of Waveguide Section (mm) | | | | | Height h (mm) | Midband Frequency (GHz) | ± 1dB Bandwidth of the Coupling (GHz) | Isolation (dB) | Return Loss (dB) |
|---|---|---|---|---|---|---|---|---|---|---|---|---|---|---|---|---|---|
| | | | $S_1=S_N$ | $S_2=S_{N-1}$ | $S_3=S_{N-2}$ | $S_4=S_{N-3}$ | $S_5=S_{N-4}$ | $L_0=L_N$ | $L_1=L_{N-1}$ | $L_2=L_{N-2}$ | $L_3=L_{N-3}$ | $L_4=L_{N-4}$ | | | | | |
| -3 | 5 | 0.2 | 0.735 | 0.752 | 0.730 | | | 1) | 7.999 | 0.642 | | | 0 | 11.25 | 0.3 | 35 | 35 |
| -4.77 | 3 | 0.2 | 0.555 | 1.216 | | | | 1) | 7.996 | | | | 0 | 11.25 | 0.3 | 30 | 30 |
| -4.77 | 6 | 0.2 | 0.385 | 0.274 | 0.199 | | | 1) | 8.999 | 0.669 | 3.048 | | 0 | 11.25 | 0.3 | 38 | 38 |
| -4.77 | 9 | 0.2 | 0.166 | 0.106 | 0.200 | 0.118 | 0.182 | 1) | 7.514 | 0.407 | 6.080 | 0.334 | 0 | 11.25 | 0.3 | 40 | 40 |

1) cf., footnote Table I.

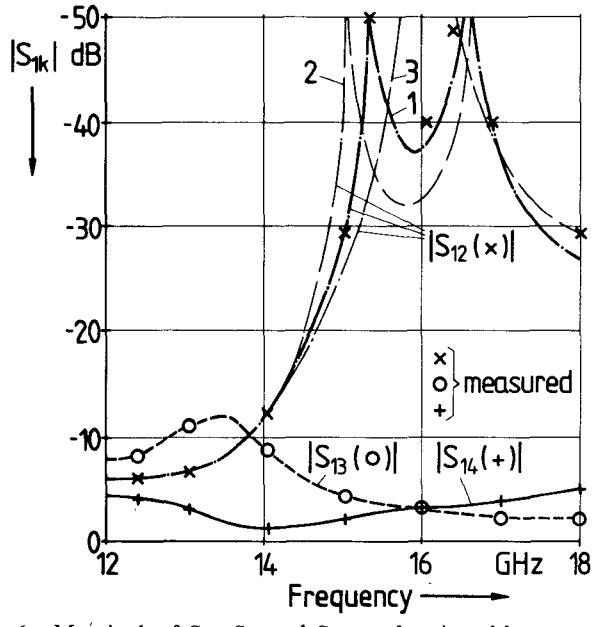


Fig. 6. Magnitude of $S_{12}$, $S_{13}$, and $S_{14}$ as a function of frequency for a computer-optimized simple *Ku*-band four-slot coupler (cf., Table III). Coupling sheet-metal thickness $t=150$ $\mu$m, step height $h=0$ mm. Influence on $|S_{12}|$ due to etching errors (lengths of the coupling slots all longer or shorter by $\Delta l$):

1 $\Delta l = 0$
2 $\Delta l = +70$ $\mu$m
3 $\Delta l = -70$ $\mu$m

(the curves of $|S_{11}|$ are omitted for clearness because they show similar behavior to $|S_{12}|$).

*Scattering Matrix Elements in (5)*

$$S_{11mn}^{H\,mq} = \sqrt{\frac{|k_{zmn}^{I}|}{|k_{zmq}^{I}|}} \cdot A_{mn}^{Imq(\mathrm{I})}$$

$$S_{12mn}^{H\,mq} = \sqrt{\frac{|k_{zmn}^{I}|\cdot b_1}{|k_{zmq}^{II}|\cdot b_2}} \cdot A_{mn}^{Imq(\mathrm{II})}$$

$$S_{21mn}^{H\,mq} = \sqrt{\frac{|k_{zmn}^{II}|\cdot b_2}{|k_{zmq}^{I}|\cdot b_1}} \cdot B_{mn}^{IImq(\mathrm{I})}$$

$$S_{22mn}^{H\,mq} = \sqrt{\frac{|k_{zmn}^{II}|}{|k_{zmq}^{II}|}} \cdot B_{mn}^{IImq(\mathrm{II})} \qquad \text{(A2)}$$

Fig. 7. Photograph of the metal insert containing the metal-etched coupling slots for the *Ku*-band four-slot coupler of Fig. 6. Material: 99.9-percent pure copper, insert thickness $t=150$ $\mu$m.

where the superscripts $mq$ denote the exciting mode, the subscripts $mn$ the excited mode, respectively. The amplitude coefficients $A$ and $B$ are given by

$$\left(\begin{array}{ccc|ccc} A_{m0}^{Im0(\mathrm{I})} & \cdots & A_{m0}^{ImN(\mathrm{I})} & A_{m0}^{Im0(\mathrm{II})} & \cdots & A_{m0}^{ImN(\mathrm{II})} \\ \vdots & & & \vdots & & \\ A_{mN}^{Im0(\mathrm{I})} & \cdots & A_{mN}^{ImN(\mathrm{I})} & A_{mN}^{Im0(\mathrm{II})} & \cdots & A_{mN}^{ImN(\mathrm{II})} \\ \hline B_{m0}^{IIm0(\mathrm{I})} & \cdots & B_{m0}^{IImN(\mathrm{I})} & B_{m0}^{IIm0(\mathrm{II})} & \cdots & B_{m0}^{IImN(\mathrm{II})} \\ \vdots & & \vdots & \vdots & & \\ B_{mN}^{IIm0(\mathrm{I})} & \cdots & B_{mN}^{IImN(\mathrm{I})} & B_{mN}^{IIm0(\mathrm{II})} & \cdots & B_{mN}^{IImN(\mathrm{II})} \end{array}\right) = (F)^{-1}\cdot(G) \qquad \text{(A3)}$$

$$(F) = \left(\begin{array}{c|cc} (U) & -(e_{nk}) & \\ \hline & k_{zm0}^{\mathrm{II}} & 0 \\ (k_{zmn}^{\mathrm{I}}\cdot f_{kn}) & & \ddots \\ & 0 & k_{zmN}^{\mathrm{II}} \end{array}\right)$$

$$(G) = \left(\begin{array}{c|cc} -(U) & (e_{nk}) & \\ \hline & k_{zm0}^{\mathrm{II}} & 0 \\ (k_{zmn}^{\mathrm{I}}\cdot f_{kn}) & & \ddots \\ & 0 & k_{zmN}^{\mathrm{II}} \end{array}\right)$$

where $(U)$ = unity matrix, and, e.g., $A_{m1}^{Im2(\mathrm{I})}$ denotes the amplitude coefficient $A^{\mathrm{I}}$ of the $\mathrm{TE}_{m1}^{x}$-wave reflected in the subregion I excited by a $\mathrm{TE}_{m2}^{x}$-wave incident in the subregion I (cf., Fig. 2(b)) with the amplitude $D^{\mathrm{I}}=1$; $B_{m3}^{IIm0(\mathrm{I})}$ denotes the amplitude coefficient $B^{\mathrm{II}}$ of the $\mathrm{TE}_{m3}^{x}$-wave transmitted in the subregion II excited by a $\mathrm{TE}_{m0}^{x}$-wave incident in the subregion I with the amplitude $D^{\mathrm{I}}=1$; etc.

*Standing-Wave Expression $\Psi_{mn}^{ci}(z)$ in (6) (cf., Fig. 2(c))*

Case 1 ($c1$):

$$H_t = 0 \text{ (magnetic wall) at } w_1 \ (z = l_1)$$
$$E_t = 0 \text{ (electric wall) at } w_2 \ (y = b_3)$$
$$\Psi_{mn}^{c1}(z) = \sin k_{zmn}^{\mathrm{III}}(z - l_1)$$
$$k_y^{III} = \frac{n\pi}{b_3}, \qquad k_{zmn}^{\mathrm{III}}: \text{ cf.(2).} \tag{A4}$$

Case 2 ($c2$):

$$E_t = 0 \text{ (electric wall) at } w_1 \ (z = l_1)$$
$$E_t = 0 \text{ (electric wall) at } w_2 \ (y = b_3)$$
$$\Psi_{mn}^{c2}(z) = \cos k_{zmn}^{\mathrm{III}}(z - l_1)$$
$$k_y^{\mathrm{III}} = \frac{n\pi}{b_3}. \tag{A5}$$

Case 3 ($c3$):

$$H_t = 0 \text{ (magnetic wall) at } w_1 (z = -l_1)$$
$$H_t = 0 \text{ (magnetic wall) at } w_2 \ (y = b_3)$$
$$\Psi_{mn}^{c3} = \sin k_{zmn}^{\mathrm{III}}(z - l_1)$$
$$k_y^{\mathrm{III}} = \frac{(2n+1)}{2} \cdot \frac{\pi}{b_3}. \tag{A6}$$

Case 4 ($c4$):

$$E_t = 0 \text{ (electric wall) at } w_1 \ (z = -l_1)$$
$$H_t = 0 \text{ (magnetic wall) at } w_2 \ (y = b_3)$$
$$\Psi_{mn}^{c4} = \cos k_{zmn}^{\mathrm{III}}(z - l_1)$$
$$k_y^{\mathrm{III}} = \frac{(2n+1)}{2} \cdot \frac{\pi}{b_3}. \tag{A7}$$

*Relations of the Amplitude Coefficients in (6) due to Field Matching for the Four Boundary Cases*

Case 1:

$$+ jk_{zmi}^{\mathrm{III}} \cos\left(-k_{zmi}^{\mathrm{III}} l_1\right) B_{mi}^{\mathrm{III}} = \sum_{n=0}^{N} \left(A_{mn}^{\mathrm{II}} - D^{\mathrm{II}}\delta_{qn}\right) f_{in1}$$
$$A_{mi}^{\mathrm{II}} + D^{\mathrm{II}}\delta_{qi} = \sum_{n=0}^{N} \sin\left(-k_{zmn}^{\mathrm{III}} l_1\right) B_{mn}^{\mathrm{III}} e_{in1}, \tag{A8}$$

Case 2:

$$- jk_{zmi}^{\mathrm{III}} \sin\left(-k_{zmi}^{\mathrm{III}} l_1\right) B_{mi}^{\mathrm{III}} = \sum_{n=0}^{N} \left(A_{mn}^{\mathrm{II}} - D^{\mathrm{II}}\delta_{qn}\right) f_{in2}$$
$$A_{mi}^{\mathrm{II}} + D^{\mathrm{II}}\delta_{qi} = \sum_{n=0}^{N} \cos\left(-k_{zmn}^{\mathrm{III}} l_1\right) B_{mn}^{\mathrm{III}} e_{in2}, \tag{A9}$$

Case 3:

$$+ jk_{zmi}^{\mathrm{III}} \cos\left(-k_{zmi}^{\mathrm{III}} l_1\right) B_{mi}^{\mathrm{III}} = \sum_{n=0}^{N} \left(A_{mn}^{\mathrm{II}} - D^{\mathrm{II}}\delta_{qn}\right) f_{in3}$$
$$A_{mi}^{\mathrm{II}} + D^{\mathrm{II}}\delta_{qi} = \sum_{n=0}^{N} \sin\left(-k_{zmn}^{\mathrm{III}} l_1\right) B_{mn}^{\mathrm{III}} e_{in3}, \tag{A10}$$

Case 4:

$$- jk_{zmi}^{\mathrm{III}} \sin\left(-k_{zmi}^{\mathrm{III}} l_1\right) B_{mi}^{\mathrm{III}} = \sum_{n=0}^{N} \left(A_{mn}^{\mathrm{II}} - D^{\mathrm{II}}\delta_{qn}\right) f_{in4}$$
$$A_{mi}^{\mathrm{II}} + D^{\mathrm{II}}\delta_{qi} = \sum_{n=0}^{N} \cos\left(-k_{zmn}^{\mathrm{III}} l_1\right) e_{in4}. \tag{A11}$$

The coupling integrals in (A8)–(A11) are given by

$$f_{in1} = f_{in2} = k_{zmn}^{\mathrm{II}} \cdot \frac{\int_0^{b_1} \frac{1}{\sqrt{1+\delta_{0i}}} \cos\left(\frac{i\pi}{b_2} y\right) \frac{1}{\sqrt{1+\delta_{0n}}} \cos\left(\frac{n\pi}{b_1} y\right) dy}{\int_0^{b_2} \frac{1}{1+\delta_{0i}} \cos^2\left(\frac{i\pi}{b_2} y\right) dy} \tag{A12}$$

$$e_{in1} = e_{in2} = \frac{\int_0^{b_1} \frac{1}{\sqrt{1+\delta_{0i}}} \cos\left(\frac{i\pi}{b_1} y\right) \frac{1}{\sqrt{1+\delta_{0n}}} \cos\left(\frac{n\pi}{b_2} y\right) dy}{\int_0^{b_1} \frac{1}{1+\delta_{0i}} \cos^2 \frac{i\pi}{b_1} y \, dy} \tag{A13}$$

$$f_{in3} = f_{in4} = k_{zmn}^{\mathrm{II}} \cdot \frac{\int_0^{b_1} \frac{1}{\sqrt{1+\delta_{0i}}} \cos\left(\frac{2i+1}{2b_2}\pi y\right) \frac{1}{\sqrt{1+\delta_{0n}}} \cos\left(\frac{n\pi}{b_1} y\right) dy}{\int_0^{b_2} \frac{1}{1+\delta_{0i}} \cos^2\left(\frac{2i+1}{2b_2}\pi y\right) dy} \tag{A14}$$

$$e_{in3} = e_{in4} = \frac{\int_0^{b_1} \frac{1}{\sqrt{1+\delta_{0i}}} \cos\left(\frac{i\pi}{b_1} y\right) \frac{1}{\sqrt{1+\delta_{0n}}} \cos\left(\frac{2n+1}{2b_2}\pi y\right) dy}{\int_0^{b_1} \cos^2\left(\frac{i\pi}{b_1} y\right) dy}. \tag{A15}$$

The input reflection coefficient $S_{1p}^{ci}$ in (9) is given by

$$S_{1pmn}^{cimq} = \sqrt{\frac{|k_{zmn}^{II}|}{|k_{qmz}^{II}|}} \cdot A_{mn}^{IImq(II)} \Bigg|_{ci}$$

for the four boundary cases $c1, \cdots, c4$. $A_{mn}^{IImq(II)}$ is the amplitude coefficient $A^{II}$ of the $TE_{mn}^{x}$-wave reflected in the subregion II excited by a $TE_{mq}^{x}$-wave incident in the subregion II with the amplitude $D^{II}=1$. This coefficient is given by (A8)–(A11), using the matrix notation, analogous to (A3), for the four boundary cases.

## References


[1] N. Marcuvitz, *Waveguide Handbook*. New York: McGraw-Hill, 1951, pp. 373–375.

[2] L. Young, "Branch guide directional couplers," in *Proc. Nat. Electron. Conf. 12*, 1956, pp. 723–732.

[3] J. Reed and G. J. Wheeler, "A method of analysis of symmetrical four-port networks," *IRE Trans. Microwave Theory Tech.*, vol. MTT-4, pp. 246–252, 1956.

[4] J. Reed, "The multiple branch waveguide coupler," *IRE Trans. Microwave Theory Tech.*, vol. MTT-6, pp. 390–403, 1958.

[5] K. G. Patterson, "A method for accurate design of a broad-band multibranch waveguide coupler," *IRE Trans. Microwave Theory Tech.*, vol. MTT-7, pp. 466–473, 1959.

[6] L. Young, "Synchronous branch-guide directional couplers for low and high power applications," *IRE Trans. Microwave Theory Tech.*, vol. MTT-10, pp. 459–475, Nov. 1962.

[7] G. L. Mathaei, L. Young, and E. M. T. Jones, *Microwave Filters, Impedance-Matching Networks, and Coupling Structures*. New York: McGraw-Hill, 1964.

[8] R. Levy, "Directional couplers," in *Advances in Microwaves*, vol. 1, L. Young, Ed. New York: Academic, 1966, pp. 155–161.

[9] R. Levy and L. F. Lind, "Synthesis of symmetrical branch-guide directional couplers," *IEEE Trans. Microwave Theory Tech.*, vol. MTT-16, pp. 80–89, 1968.

[10] R. Levy, "Analysis of practical branch-guide directional couplers," *IEEE Trans. Microwave Theory Tech.*, vol. MTT-17, pp. 289–290, 1969.

[11] H. J. Riblet, "Comment on 'Synthesis of symmetrical branch-guide directional couplers,'" *IEEE Trans. Microwave Theory Tech.*, vol. MTT-18, pp. 47–48, 1970.

[12] M. F. Bottjer and H. E. King, "Top-wall and branch-waveguide hybrids for millimeter wavelengths," *IEEE Trans. Microwave Theory Tech.*, vol. MTT-20, pp. 182–184, 1972.

[13] R. Levy, "Zolotarev branch-guide couplers," *IEEE Trans. Microwave Theory Tech.*, vol. MTT-21, pp. 95–99, 1973.

[14] E. Kühn, "Improved design and resulting performance of multiple branch-waveguide directional couplers," *Arch. Elec. Übertragung*, vol. 28, pp. 206–214, 1974.

[15] F. Arndt, D. Ellermann, H. W. Häusler, and J. Strube, "Field theory analysis and numerical synthesis of symmetrical multiple-branch waveguide couplers," *Frequenz*, vol. 36, pp. 262–266, 1982.

[16] R. Vahldieck, J. Bornemann, F. Arndt, and D. Grauerholz, "Optimized waveguide *E*-plane metal insert filters for millimeter-wave applications," *IEEE Trans. Microwave Theory Tech.*, vol. MTT-31, pp. 65–69, Jan. 1983.

[17] R. Vahldieck, J. Bornemann, F. Arndt, and D. Grauerholz, "*W*-band low-insertion-loss *E*-plane filter," *IEEE Trans. Microwave Theory Tech.*, vol. MTT-32, pp. 133–135, Jan. 1984.

[18] R. E. Collin, *Field Theory of Guided Waves*. New York: McGraw-Hill, 1960, pp. 338–348, 171–179, 85–87.

[19] R. F. Harrington, *Time Harmonic Electromagnetic Fields*. New York: McGraw-Hill, 1961, pp. 171–177.

[20] A. Wexler, "Solution of waveguide discontinuities by modal analysis," *IEEE Trans. Microwave Theory Tech.*, vol. MTT-15, pp. 508–517, Sept. 1967.

[21] H. Patzelt and F. Arndt, "Double plane steps in rectangular waveguides and their application for transformers, irises, and filters," *IEEE Trans. Microwave Theory Tech.*, vol. MTT-30, pp. 771–776, May 1982.



**Fritz Arndt** (SM'83) was born in Konstanz, Germany, on April 30, 1938. He received the Dipl.-Ing., the Dr.-Ing., and the Habilitation degrees from the Technical University of Darmstadt, Germany, in 1963, 1968, and 1972, respectively.

From 1963 to 1972, he worked on directional couplers and microstrip techniques at the Technical University of Darmstadt. Since 1972, he has been a Professor and Head of the Microwave Department at the University of Bremen, Germany. His research activities are at present in the area of the solution of field problems of waveguide, finline, and optical waveguide structures, of antenna design, and of scattering structures.

Dr. Arndt is member of the VDE and NTG (Germany). In 1970, he received the NTG award, in 1982 the A. F. Bulgin Award (together with three coauthors) from the Institution of Radio and Electronic Engineers.


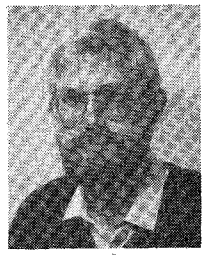


**Bernd Koch** was born in Brunsbüttelkoog, West Germany, on January 12, 1959. He received the Dipl.-Ing. degree from the University of Bremen, West Germany, 1983. He worked on directional couplers at the University of Bremen.

Since 1984, he has been a member of the German Airforce.


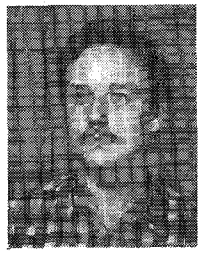


**Hans-Joachim Orlok** was born in Emden, West Germany, on July 25, 1955. He received the Dipl.-Ing. degree from the University of Bremen, West Germany, 1983. He worked on directional couplers at the University of Bremen.

Since 1984, he has been a development engineer with Elektro Spezial Bremen/Phillips, West Germany.


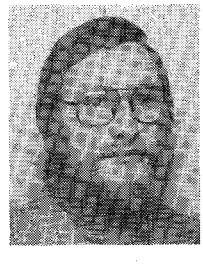


**Norbert Schröder** was born in Iserlohn, West Germany, on June 22, 1957. He received the Dipl.-Ing. degree from the University of Bremen, West Germany, 1983. He worked on directional couplers at the University of Bremen.

Since 1984, he has been a development engineer on microwave components and antennas with MBB/ERNO GmbH, West Germany.